Oral Radiol (2016) 32:14–21
DOI 10.1007/s11282-015-0205-9

ORIGINAL ARTICLE

CT and MRI findings of primitive neuroectodermal tumor in the maxillofacial region

Hong-jun Hou[1] · Zu-shan Xu[1] · Dong Xu[1] · Hong-sheng Zhang[1] · Jie Liu[1] · Wen-jun Zhang[1]

Received: 19 September 2014 / Accepted: 8 February 2015 / Published online: 19 March 2015

Abstract
Objectives To summarize the computed tomography (CT) and magnetic resonance imaging (MRI) findings of rare primitive neuroectodermal tumors (PNETs) in the maxillofacial region.
Methods The clinical data, and CT and MRI findings of seven patients with pathologically proven PNETs in the maxillofacial region were retrospectively reviewed. The patients comprised five males and two females with a mean age of 16.4 years. The tumor location, size, margin, CT attenuation or signal intensity, contrast enhancement characteristics, and involvement of adjacent tissues were assessed.
Results There were a total of seven tumors. Four lesions were located in the masticator space. The lesions were seen as ill-defined ($n = 6$) or well-defined ($n = 1$) aggressive masses with a mean size of 5.6 cm. Bone destruction was found in six patients. The density or signal enhancement patterns of the lesions were heterogeneous, with necrosis seen in all seven tumors. Calcification and regional enlarged lymph nodes were not seen in any patients.
Conclusions A large, ill-defined, and aggressive mass in the maxillofacial region of a young patient, associated with heterogeneous density or signal intensity but lack of calcification and regional lymphadenopathy, may suggest a diagnosis of PNET.

✉ Zu-shan Xu
xuzushan@sohu.com

[1] Department of Radiology, Wendeng Center Hospital of Weihai, No. 3 Mishan East Road, Wendeng District, Weihai 264400, Shandong, China

Keywords Primitive neuroectodermal tumor · Tomography · X-ray computed · Magnetic resonance imaging

Introduction

Primitive neuroectodermal tumor (PNET), encompassing central PNET and peripheral PNET, is a rare, highly malignant, small round-cell tumor [1]. Peripheral PNET is commonly related to Ewing's sarcoma and expresses large amounts of CD99 [2]. Peripheral PNET is frequently reported to be located in the thoracic region, pelvis, abdominal region, limbs, and spine [3–7]. The incidence of head and neck PNET varies from 0–42 % [8–10]. The most common location for head and neck PNET is the orbit, followed by the neck and the parotid gland [9]. PNET arising from the maxillofacial region is extremely rare. Only sporadic cases have been reported to date [1, 9, 11], and most of these reports focused on the clinicopathological features, treatment, and prognosis of PNET. Reports on the imaging features of PNET in the maxillofacial region are limited.

In this study, we retrospectively analyzed the computed tomography (CT) and magnetic resonance imaging (MRI) findings for seven patients with pathologically proven PNET in the maxillofacial region. The purpose was to summarize the CT and MRI findings of this rare type of tumor in the maxillofacial region.

Materials and methods

Patients

Seven consecutive patients with histologically proven PNET in the maxillofacial region between July 2004 and September 2013 were included. This study received

approval from our institutional review board, and informed consent from the patients was not required because of the retrospective nature of the study. The patients were five males and two females, with an age range of 4–32 years and a mean age of 16.4 years. The main symptoms included swelling ($n = 6$), pain and tenderness ($n = 5$), nasal epistaxis ($n = 1$), and nasal obstruction ($n = 2$). The symptom duration ranged from 1–14 months, with a mean of 5.6 months. Four patients underwent complete surgical excision, two patients underwent incomplete surgical excision, and one patient underwent a biopsy only. After surgical treatment, four patients received systemic chemotherapy plus local radiotherapy, and two patients received systemic chemotherapy. The remaining patient received systemic chemotherapy plus radiotherapy after the biopsy. During follow-up for 9 months to 5 years, three patients had local recurrence and two patients developed distant metastasis to the lung, liver, or bone. Two patients had no evidence of disease during a 3- to 5-year follow-up period, two patients died of distant metastasis at 26 and 42 months after diagnosis, and three patients remained alive with disease during follow-up of 9 months to 2 years. The detailed clinical profiles of the patients are shown in Table 1.

CT and MRI

One patient underwent CT examination, five patients underwent MRI examination, and one patient underwent both CT and MRI examinations. Unenhanced and contrast-enhanced CT or MRI was performed in all patients. CT images were obtained with a 16-slice spiral CT (Somatom VolumeZoom; Siemens Medical Systems, Forchheim, Germany). The main scan parameters included tubular voltage of 120 kV, tubular current of 250 mA, field of view of 240 mm, pitch of 1.2, and matrix of 512 × 512. Thin slice images (1-mm section thickness) were reconstructed with no overlap using a smooth and sharp kernel for interpretation. Contrast-enhanced images were obtained at 30–35 s after intravenous injection of Iopamidol (Ultravist 300; Schering, Berlin, Germany) with a dosage of 1.5 ml/kg body weight at a rate of 3 ml/s. MRI images were obtained using a 1.5 T superconductive unit (Achieva; Philips Medical Systems, Best, The Netherlands) ($n = 4$) or a 3.0 T superconductive unit (Discovery MR 750; General Electric, Milwaukee, WI) ($n = 2$). The sequences included transverse spin-echo T1-weighted imaging (TR/TE = 450 ms/15 ms), and transverse and coronal fast spin-echo T2-weighted imaging (TR/TE = 3500 ms/120 ms). The remaining parameters included field of view of 230 mm × 230 mm for transverse imaging and 250 mm × 250 mm for coronal imaging, matrix of 256 × 256, and slice thickness/gap ratio of 5 mm/0.5 mm. Contrast-enhanced transverse, coronal, and sagittal T1-weighted images were obtained after intravenous injection of gadopentetate dimeglumine (Magnevist; Schering) with a dosage of 0.2 mmol/kg body weight at a rate of 2.5 ml/s.

Imaging analysis

All images were evaluated by two experienced radiologists (D. X. and H. Z. with 7 and 10 years of experience in diagnostic imaging, respectively) by consensus. The tumor location, size, margin (well-defined or ill-defined), signal intensity (relative to the cerebral cortex) and CT density (compared with adjacent muscle), pattern and degree of contrast enhancement, and involvement of adjacent tissues were assessed. Patterns of enhancement were categorized as homogeneous or heterogeneous. Degrees of enhancement on CT or MR images were evaluated separately, and graded as mild, moderate, and intense compared with the adjacent muscle and mucosa. The grades were defined as

Table 1 Clinical profiles of seven patients with PNET in the maxillofacial region

Case no.	Age (years)	Sex	Clinical presentation	Symptoms duration (mo)	Treatment	Distant metastasis	Recurrence	Follow-up period (mo)	Outcome
1	4	M	Swelling, pain, and nasal obstruction	4	SE + ChT + RT	(−)	(+)	9	AWD
2	26	M	Swelling and pain	1	SE + ChT	(−)	(+)	16	AWD
3	32	M	Swelling and pain	3	SE + ChT	(−)	(+)	24	AWD
4	17	F	Swelling	4	SE + ChT + RT	(−)	(−)	36	NED
5	12	M	Swelling and pain	5	SE + ChT + RT	(−)	(−)	60	NED
6	11	F	Nasal epistaxis and nasal obstruction	14	SE + ChT + RT	Lung and liver	(−)	42	Dead
7	13	M	Swelling and pain	8	ChT + RT	Lung and bone	NA	26	Dead

SE surgical excision, *ChT* chemotherapy, *RT* radiation therapy, (−) negative, (+) positive, *NA* not applicable, *NED* no evidence of disease, *AWD* alive with disease

follows: mild if the attenuation on CT images or lesion signal intensity on MR images was lower than or similar to that of the muscle; moderate if they were greater than that of the muscle but lower than that of the mucosa; and intense if they were similar to or greater than that of the mucosa. The radiological features of cervical lymphadenopathy were also evaluated. The diagnosis of node involvement was defined according to previously reported central necrosis and size criteria [12].

Histopathology

The resected tumors ($n = 6$) or biopsy samples ($n = 1$) were processed for conventional hematoxylin–eosin staining and immunohistological staining. Histologically, all tumors were composed of nests and sheets of small round cells with scant cytoplasm, well-defined nuclei, and distinct nucleoli. The tumor cells were arranged around a central core of neurofibrillary material and formed Homer–Wright rosettes in two patients. Microscopic evidence of bone invasion was found in five patients. Immunohistochemically, CD99 was positive in all tumors. Regarding neural markers, neuron-specific enolase was positive in six patients, S-100 was positive in four patients, and synaptophysin was positive in four patients. All cases were positive for at least two neural markers. In addition, all tumors were positive for vimentin and negative for cytokeratin and actin. The detailed histological and immunohistochemical characteristics of the lesions are shown in Table 2.

Results

All patients had a unilateral and solitary tumor. There were a total of seven tumors. The CT and MRI findings of the seven tumors are summarized in Table 3. All lesions manifested as ill-defined ($n = 6$) or well-defined ($n = 1$) masses in various locations with irregular shapes. The most common lesion location was the masticator space ($n = 4$; Fig. 1), followed by the maxillary sinus ($n = 2$; Fig. 2), sphenoid sinus ($n = 1$; Fig. 3), submandibular space ($n = 1$; Fig. 4), nasal cavity ($n = 2$), parapharyngeal space ($n = 1$), parotid space ($n = 1$), and cheek ($n = 1$). The maximum diameter of the lesions ranged from 3.2–7.6 cm, with a mean diameter of 5.6 cm. The maximum diameter was greater than 3 cm in all patients and greater than 5 cm in five patients (71.4 %, 5/7).

On CT images, the lesions of the two patients with CT scans showed slight hypodensity and isodensity. Intratumoral calcification was not found. The margin was ill-defined in the two patients. Bone destruction was found in both lesions, with bone involvement in the mandibular ramus and sphenoid bone. Radial periosteal reaction around the mandibular ramus was found in one lesion (Fig. 4c), while the other lesion involving the sphenoid bone did not have periosteal reaction. On contrast-enhanced CT images, one lesion showed moderate enhancement and the other lesion showed intense enhancement. The pattern of enhancement was heterogeneous, and spotty or scattered necrotic areas were found in both lesions.

On MR images, the lesions of the six patients with MRI examinations showed slight hypointense signals in four

Table 2 Detailed histological and immunohistochemical findings of the seven lesions

Case no.	Histological findings	Immunohistochemical findings		Necrosis/cyst formation
		Positive	Negative	
1	Nests and sheets of small round cells with scant cytoplasm	CD99, NSE, Syn, Vimentin	CK, CK5, S-100, LCA, HMB45, CgA, CD3, Actin	Present
2	Nests and sheets of small round cells with scant cytoplasm; rosette formation	CD99, NSE, S-100, Vimentin	CK, CK5, Actin, LCA, Desmin, CD56, CK8/18, CgA, CD3, P63	Present
3	Nests and sheets of small round cells with scant cytoplasm	CD99, NSE, Vimentin, Syn, CD56	CK, Actin, LCA, SMA, CgA, Myogenin	Present
4	Nests and sheets of small round cells with scant cytoplasm	CD99, NSE, S-100, Vimentin, CD56	CK, Actin, CgA, Syn, LCA, NF, Myoglobin	Present
5	Nests and sheets of small round cells with scant cytoplasm	CD99, NSE, S-100, Vimentin, CD56	CK, Actin, Syn, LCA, Desmin, CK8/18, CgA, P63	Present
6	Nests and sheets of small round cells with scant cytoplasm; rosette formation	CD99, NSE, Syn, Vimentin	CK, CK8/18, CgA, LCA, Actin, SMA, CD56	Present
7	Nests and sheets of small round cells with scant cytoplasm	CD99, S-100, Syn, Vimentin	CK, CK5, Actin, LCA, CD3, SMA	NA

NSE neuron-specific enolase, *Syn* synaptophysin, *CK* cytokeratin, *CgA* chromogranin A, *SMA* smooth muscle actin, *LCA* leukocyte common antigen, *NF* neurofilament, *NA* not applicable

Table 3 CT and MRI findings of PNET in the maxillofacial region

Case no.	Imaging modality	Location	Size (cm)	Margin	Density	T1WI	T2WI	Enhancement	Bone destruction	Necrotic areas
1	MRI	Right maxillary sinus and nasal cavity	4.2 × 4.1	Well-defined	NA	Isointense	Hyperintense	Heterogeneous/intense	No	Yes
2	CT	Right submandibular and masticator space	6.0 × 4.8	Ill-defined	Isodense	NA	NA	Heterogeneous/moderate	Yes	Yes
3	MRI + CT	Sphenoid sinus	3.2 × 3.0	Ill-defined	Hypodense	Hypointense	Hyperintense	Heterogeneous/intense (MRI) Heterogeneous/intense (CT)	Yes	Yes
4	MRI	Left masticator space	7.3 × 6.1	Ill-defined	NA	Isointense	Hyperintense	Heterogeneous/moderate	Yes	Yes
5	MRI	Right masticator space	5.6 × 4.7	Ill-defined	NA	Hypointense	Isointense	Heterogeneous/intense	Yes	Yes
6	MRI	Right maxillary sinus, nasal cavity, and palate	5.2 × 3.6	Ill-defined	NA	Hypointense	Hyperintense	Heterogeneous/moderate	Yes	Yes
7	MRI	Right masticator space Parapharyngeal space, parotid space, and cheek	7.6 × 5.6	Ill-defined	NA	Hypointense	Hyperintense	Heterogeneous/intense	Yes	Yes

T1WI T1-weighted imaging, *T2WI* T2-weighted imaging, *NA* not applicable

patients and isointense signals in two patients on T1-weighted images, and hyperintense signals in five patients and isointense signals in one patient on T2-weighted images. The margin was ill-defined in five lesions and well-defined in one lesion. On contrast-enhanced MR images, two lesions showed moderate enhancement and four lesions showed intense enhancement. The pattern of enhancement was heterogeneous, and spotty or scattered necrotic areas were found in all six lesions. All six lesions invaded the adjacent soft tissues, and one lesion extended into the intracranial cavity. Cervical lymphadenopathy was not found in any patients.

Discussion

Since its initial description in 1918 [13], PNET is now regarded as a type of Ewing family tumor and as a related entity to Ewing's sarcoma. The common features of PNET and Ewing's sarcoma are malignant, small round-cell tumors with strong expression of the surface glycoprotein p30/32 (CD99) [14]. The distinction between these tumors is mainly based on the presence of typical Homer–Wright rosettes and/or neural differentiation [2]. PNET is commonly positive for at least two different neural markers, such as neuron-specific enolase, synaptophysin, or S-100 [2]. In our series, all tumors were positive for CD99 and positive for at least two neural markers. Homer–Wright rosettes were present in two patients. These findings confirmed the diagnosis of PNET histologically.

PNET located in the maxillofacial region is extremely rare. In a series of 11 cases of PNET, just two patients were reported have tumors in the head and neck region [6]. Clinically, PNET is seen in a wide age range from newborn to 74 years, with a mean age of 21 years, and has a predilection for children and adolescents. The sex distribution of patients has varied among different studies [9, 10, 15], but most series showed a male predominance [10, 15]. These findings were consistent with our cases. Moreover, in our series, the masticator space was the most commonly involved location for maxillofacial PNET. A standard protocol for managing PNET has not yet been established, and the prognosis of PNET is generally poor because of its obviously aggressive nature, and malignant biological and clinical characters. Most patients develop recurrence and distant metastasis after initial treatment. The disease-free survival rate was reported to be approximately 50 % at 3 years and 30–45 % at 5 years [9, 16]. In our series, most of the patients suffered from recurrence or distant metastasis after surgical excision plus chemotherapy or radiotherapy, but with a survival time of less than 4 years.

Previous reports on CT and/or MRI findings of PNET in the head and neck, chest wall, abdomen, pelvis, limbs, and

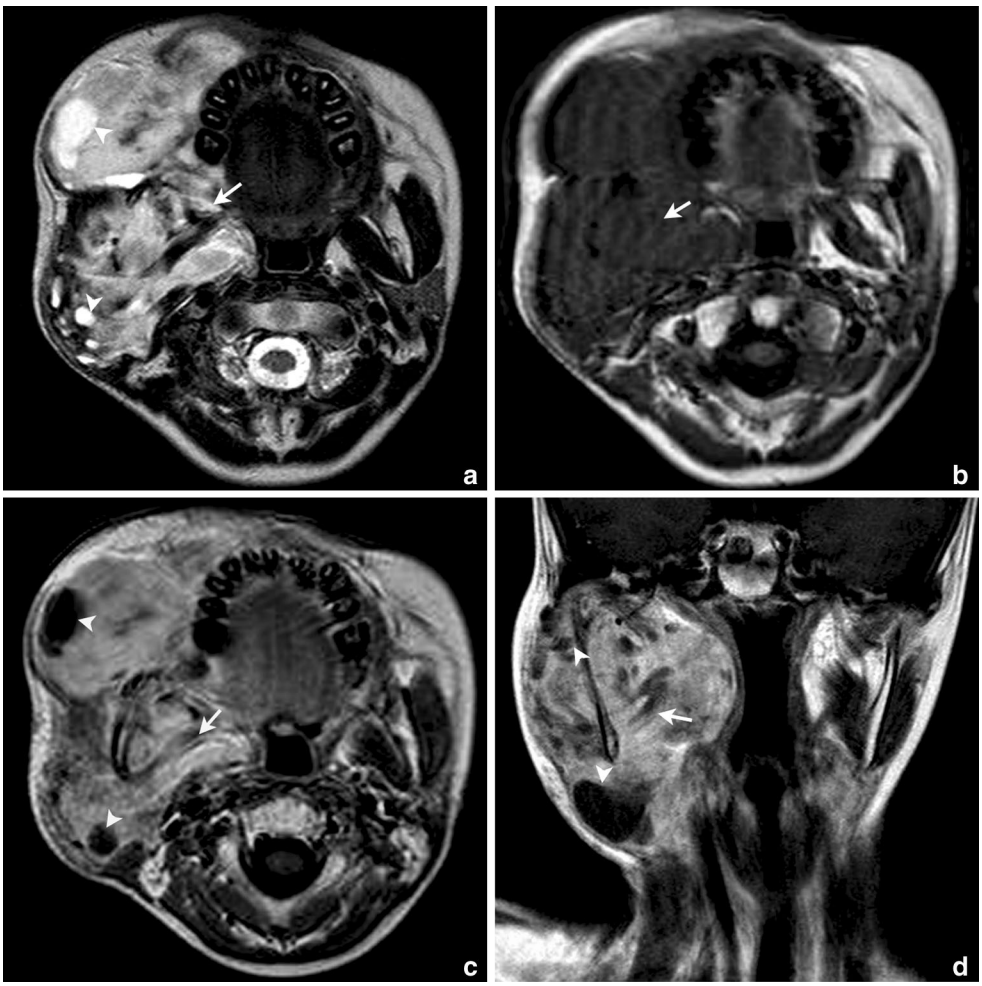

Fig. 1 PNET of the right masticator space, parapharyngeal space, parotid space, and cheek in a 13-year-old male (Case 7). **a** Axial T2-weighted image shows a large aggressive mass with heterogeneous signal hyperintensity (*arrow*) and intratumoral spotty necrotic areas (*arrowhead*). **b** Axial T1-weighted image shows a mass with hypointensity (*arrow*). **c, d** Gadolinium-enhanced axial T1-weighted image (**c**) and coronal T1-weighted image (**d**) show a mass with heterogeneous intense enhancement (*arrow*) and intratumoral spotty necrotic areas (*arrowhead*)

spine [3, 4, 11, 17, 18] showed no specific radiologic features of PNET, although CT and MRI remain valuable tools for preoperative evaluation and surgical planning for this tumor. In our series, the attenuation, signal intensity, and enhancement patterns of PNET in the maxillofacial region were also nonspecific. Furthermore, most of our cases exhibited a large, ill-defined mass with aggressive infiltration into adjacent tissues and bones, which reflected the highly malignant nature of the tumor. The most frequently involved bone was the mandibular ramus. The frequency of bone involvement in our series was higher than that in a previous study [11], wherein bone destruction was observed in two of eight patients. This might be related to the different locations of the tumors. In our series, the tumor density and signal intensity tended to be heterogeneous, with necrosis seen in all seven cases. In previous reports of PNET at other sites, necrosis was regarded as the most common radiologic finding [6, 17]. Notably, in line with the previous report of eight PNET lesions in the head and neck [11], calcification was not found in our cases. Taken together, calcification is considered a rare radiologic finding of PNET [18, 19].

The incidences of lymphadenopathy with PNET in the head and neck were previously reported to vary from 0–11.6 % [9, 18]. None of our patients showed enlarged regional lymph nodes, despite the highly aggressive and malignant features of PNET. Recently, lymphadenopathy was found to occur in 5 of 43 patients with PNET in the head and neck [9]. Nevertheless, no patients had lymphadenopathy in another report of seven patients with PNET in the head and neck [18]. Regarding PNET at other locations, local lymphadenopathy was documented in only one of eight patients with chest wall PNETs [20], and none of 14 patients with peripheral PNETs [6]. Lack of regional enlarged lymph nodes appears to be characteristic for PNET in the maxillofacial region.

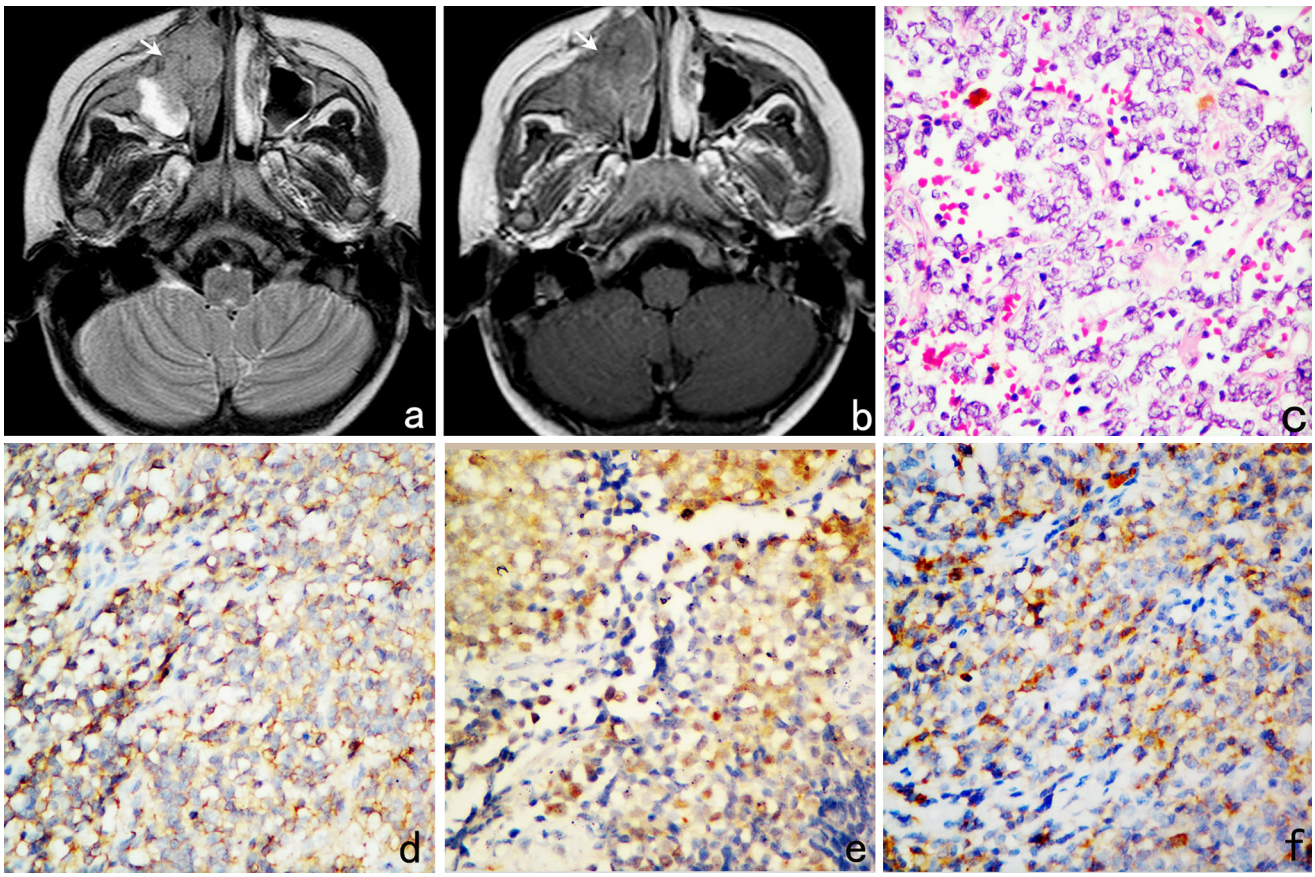

Fig. 2 PNET of the right maxillary sinus and nasal cavity in an 11-year-old female (Case 6). **a** Axial T2-weighted image shows a large aggressive mass with invasion to the right nasal cavity (*arrow*). **b** Gadolinium-enhanced axial T1-weighted image shows a mass with heterogeneous moderate enhancement (*arrow*). **c, d** Photomicrographs show a tumor composed of nests and sheets of small round cells with scant cytoplasm (**c**) (hematoxylin–eosin; magnification × 400) and positive staining for CD99 (**d**), neuron-specific enolase (**e**), and synaptophysin (**f**) (magnification × 400)

Fig. 3 PNET of the sphenoid sinus in a 32-year-old male (Case 3). **a** Axial contrast-enhanced CT image shows a mass with heterogeneous intense enhancement (*arrow*) and intratumoral necrotic areas (*arrowhead*). **b** Axial T2-weighted image shows a heterogeneous hyperintense mass (*arrow*). **c** Gadolinium-enhanced axial T1-weighted image with fat saturation shows a mass with heterogeneous intense enhancement (*arrow*)

Fig. 4 PNET of the right submandibular space and masticator space in a 26-year-old male (Case 2). **a** Axial contrast-enhanced CT image shows a large mass with heterogeneous moderate enhancement (*arrow*) and intratumoral necrotic areas (*arrowhead*). **b** Axial contrast-enhanced CT image shows a mass with heterogeneous moderate enhancement (*arrow*) and bone destruction (*arrowhead*). **c** Axial CT image on the bone window shows bone destruction of the mandibular ramus (*arrow*) with radial periosteal reaction (*arrowhead*)

In conclusion, PNET in the maxillofacial region exhibits nonspecific attenuation and signal patterns on CT or MR images. It is difficult to make a definitive diagnosis based only on CT and MR images. However, a large, ill-defined mass in the maxillofacial region with aggressive infiltration into adjacent tissues and bone destruction in a young patient, accompanied by heterogeneous enhancement caused by necrosis but no calcification or regional lymphadenopathy, may suggest a diagnosis of PNET.

Conflict of interest Hong-jun Hou, Zu-shan Xu, Dong Xu, Hongsheng Zhang, Jie Liu, and Wen-jun Zhang declare that they have no conflict of interest.

Human rights statements and informed consent All procedures followed were in accordance with the ethical standards of the responsible committee on human experimentation (institutional and national) and with the Helsinki Declaration of 1964 and later versions. Informed consent was not required in accordance with the requirements for such a retrospective study.

References

1. Windfuhr JP. Primitive neuroectodermal tumor of the head and neck: incidence, diagnosis, and management. Ann Otol Rhinol Laryngol. 2004;113:533–43.
2. de Alava E, Gerald WL. Molecular biology of the Ewing's sarcoma/primitive neuroectodermal tumor family. J Clin Oncol. 2000;18:204–13.
3. Khong PL, Chan GC, Shek TW, Tam PK, Chan FL. Imaging of peripheral PNET: common and uncommon locations. Clin Radiol. 2002;57:272–7.
4. Duan XH, Ban XH, Liu B, Zhong XM, Guo RM, Zhang F, et al. Intraspinal primitive neuroectodermal tumor: imaging findings in six cases. Eur J Radiol. 2011;80:426–31.
5. Winer-Muram HT, Kauffman WM, Gronemeyer SA, Jennings SG. Primitive neuroectodermal tumors of the chest wall (Askin tumors): CT and MR findings. AJR Am J Roentgenol. 1993;161:265–8.
6. Qian X, Kai X, Shaodong L, Gaohong C, Hong M, Jingjing L. Radiological and clinicopathological features of pPNET. Eur J Radiol. 2013;82:e888–93.
7. Jurgens H, Bier V, Harms D, Beck J, Brandeis W, Etspuler G, et al. Malignant peripheral neuroectodermal tumors. A retrospective analysis of 42 patients. Cancer. 1988;61:349–57.
8. Kimber C, Michalski A, Spitz L, Pierro A. Primitive neuroectodermal tumours: anatomic location, extent of surgery, and outcome. J Pediatr Surg. 1998;33:39–41.
9. Nikitakis NG, Salama AR, O'Malley BW Jr, Ord RA, Papadimitriou JC. Malignant peripheral primitive neuroectodermal tumor-peripheral neuroepithelioma of the head and neck: a clinicopathologic study of five cases and review of the literature. Head Neck. 2003;25:488–98.
10. Jones JE, McGill T. Peripheral primitive neuroectodermal tumors of the head and neck. Arch Otolaryngol Head Neck Surg. 1995;121:1392–5.
11. Zhang WD, Chen YF, Li CX, Zhang L, Xu ZB, Zhang FJ. Computed tomography and magnetic resonance imaging findings of peripheral primitive neuroectodermal tumors of the head and neck. Eur J Radiol. 2011;80:607–11.
12. Gor DM, Langer JE, Loevner LA. Imaging of cervical lymph nodes in head and neck cancer: the basics. Radiol Clin North Am. 2006;44:101–10, viii.
13. Stout AP. A tumor of the ulnar nerve. Proc NY Pathol Soc. 1918;21:2–12.
14. Ambros IM, Ambros PF, Strehl S, Kovar H, Gadner H, Salzer-Kuntschik M. MIC2 is a specific marker for Ewing's sarcoma and peripheral primitive neuroectodermal tumors. Evidence for a common histogenesis of Ewing's sarcoma and peripheral primitive neuroectodermal tumors from MIC2 expression and specific chromosome aberration. Cancer. 1991;67:1886–93.
15. Marina NM, Etcubanas E, Parham DM, Bowman LC, Green A. Peripheral primitive neuroectodermal tumor (peripheral neuroepithelioma) in children. A review of the St. Jude experience and controversies in diagnosis and management. Cancer. 1989;64:1952–60.
16. Schmidt D, Herrmann C, Jurgens H, Harms D. Malignant peripheral neuroectodermal tumor and its necessary distinction from Ewing's sarcoma. A report from the Kiel Pediatric Tumor Registry. Cancer. 1991;68:2251–9.
17. Kim MS, Kim B, Park CS, Song SY, Lee EJ, Park NH, et al. Radiologic findings of peripheral primitive neuroectodermal

tumor arising in the retroperitoneum. AJR Am J Roentgenol. 2006;186:1125–32.
18. Dick EA, McHugh K, Kimber C, Michalski A. Imaging of non-central nervous system primitive neuroectodermal tumours: diagnostic features and correlation with outcome. Clin Radiol. 2001;56:206–15.
19. Sallustio G, Pirronti T, Lasorella A, Natale L, Bray A, Marano P. Diagnostic imaging of primitive neuroectodermal tumour of the chest wall (Askin tumour). Pediatr Radiol. 1998;28:697–702.
20. Sabate JM, Franquet T, Parellada JA, Monill JM, Oliva E. Malignant neuroectodermal tumour of the chest wall (Askin tumour): CT and MR findings in eight patients. Clin Radiol. 1994;49:634–8.